Verification of Seismic Response Modification Factors of Uncoupled Composite Plate Shear Walls/Concrete Filled

Emre Kizilarslan, S.M.ASCE[1]; and Michel Bruneau, Dist.M.ASCE[2]

Abstract: In this paper, the seismic design factors for uncoupled composite plate shear walls/concrete filled (C-PSW/CF), a.k.a. SpeedCore, are verified by conducting a study using FEMA methodology. These are the seismic response modification factor, R, the deflection amplification factor, Cd, and the overstrength factor, Ωo; and their values for C-PSW/CF are specified as 6.5, 5.5, and 2.5, respectively. A study was needed, as these factors for uncoupled C-PSW/CFs, included in ASCE 7 since as far back as its 2000 edition, were chosen solely based on the seismic performance of similar structural systems and engineering judgment of the committee members. For this study, four archetypes with planar walls and three archetypes with C-shaped C-PSW/CF walls were chosen. Two different damage measures (DM) were chosen for this study; namely, 3% and 5% maximum interstory drifts. Based on FEMA methodology, all archetypes satisfied the specified performance requirement considering a "good" rating for total system collapse uncertainty (βTOT). **DOI: 10.1061/JSENDH.STENG-11783.**

Author keywords: Composite plate shear walls (C-PSW); Seismic response modification factors; FEMA P695 study; Inelastic behavior; Flexural behavior; Ductility; Fracture; Strength degradation.

Introduction

In this paper, the results of a FEMA P695 study (FEMA 2008) that was conducted to verify the seismic design factors for *uncoupled* Composite Plate Shear Walls/Concrete Filled (C-PSW/CF), a.k.a. SpeedCore, are presented. ASCE 7-16 (ASCE 2016) provides the seismic design factors for composite walls in row 13 of Table 12.2-1. These are the seismic response modification factor, R, the deflection amplification factor, C_d, and the overstrength factor, Ω_o, and their values for C-PSW/CF are specified as 6.5, 5.5, and 2.5, respectively. These factors for uncoupled C-PSW/CFs, included in ASCE 7 since as far back as its 2000 Edition, were chosen based on the seismic performance of similar structural systems and engineering judgment of the committee members. Therefore, the study presented here was conducted to investigate the adequacy of these seismic design factors.

FEMA P695 is a generally accepted procedure that has been developed and proposed through a consensus-based approach to establish a rigorous approach to establish the value of seismic response modification factors (such as the R-factor) that are adequate for a structural system (FEMA 2008). It relies on the use of incremental dynamic analysis (IDA) to identify the collapse threshold of such systems, as established by nonlinear time history analysis. Therefore, the credibility of the result obtained when following this procedure requires the use of nonlinear models that can adequately capture the hysteretic behavior of the yielding structural elements of the lateral load resisting system being considered. In this process, in its simplest form, the FEMA P695 approach requires such nonlinear analyses to be conducted for a prescribed set of twenty-two ground motions (that result in 44 individual ground motion records when considering orthogonal records from the same earthquake at a given station); these earthquake components are for seismic events ranging in magnitudes from M6.5 to M7.6 and are all "far field records," defined as being from sites located at distances 10 km or more from the fault rupture (PEER 2017). The procedure requires performing IDA for each of these earthquake records, which consists of repeating analysis by increasing the severity of each earthquake until collapse is reached, and repeating such analyses for a large number of archetypes (i.e., example structures), and results in many thousands nonlinear analyses. The nonlinear analysis software OpenSees was selected, as it is well suited for this purpose and permits use of macro fiber nonlinear models with rapid execution time (which would not have been the case with 2-D or 3-D finite element continuum mechanics models). OpenSees has often been used by the research community (e.g., Lignos 2008; Rodgers and Mahin 2006), particularly for IDA and FEMA P695 studies.

A similar study was done by Agrawal et al. (2020). Therefore, the same archetypes used therein were used here, to be able to compare the results. However, note that the work presented here was not conducted to replicate/repeat this previous study, but rather to reassess the adequacy of the seismic response modification factors using different non-linear modeling approaches. This is consistent with what was done in prior studies on coupled C-PSW/CFs (Bruneau et al. 2019; Kizilarslan et al. 2021b), where this was done to provide a greater confidence in the results, given the differences of opinions on how to best model C-PSW/CFs. All expert technical committees that have reviewed this prior work on coupled walls have commented positively on the benefit of considering two different sets of non-linear models. The work presented here seeks, by its complementarity to Agrawal et al. (2020), to provide the same level of confidence for uncoupled C-PSW/CFs. This is critically important given that, contrary to coupled walls, seismic energy dissipation in uncoupled walls is limited to plastic hinging at their base (barring higher mode effects that can slightly augment this). In other words,

[1]Graduate Research Assistant, Dept. of Civil Structural and Environmental Engineering, Univ. at Buffalo, Buffalo, NY 14260 (corresponding author). ORCID: https://orcid.org/0000-0003-3014-1165. Email: emrekizilarslan91@gmail.com

[2]Professor, Dept. of Civil Structural and Environmental Engineering, Univ. at Buffalo, Buffalo, NY 14260. ORCID: https://orcid.org/0000-0003-1170-468X. Email: bruneau@buffalo.edu

Note. This manuscript was submitted on June 21, 2022; approved on January 20, 2023; published online on March 29, 2023. Discussion period open until August 29, 2023; separate discussions must be submitted for individual papers. This paper is part of the ***Journal of Structural Engineering***, © ASCE, ISSN 0733-9445.

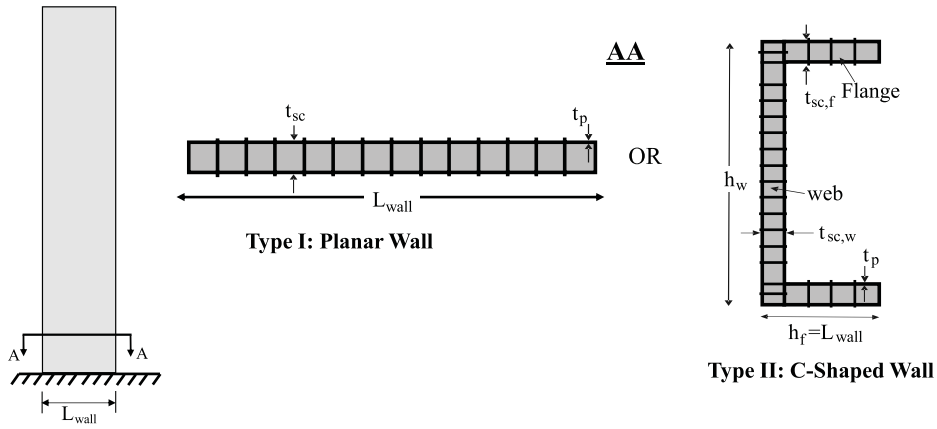

Fig. 1. Representation of archetype and two types of cross-sections of walls.

in the minds of some engineers, high R values are suspicious in cantilevering walls with inelastic energy dissipation primarily at their base, making the additional scrutiny provided here critically valuable.

Archetypes

For this study, a total of seven archetypes were considered: four with planar walls (3-story, 6-story, 9-story, and 12-story, shown as Type I in Fig. 1) and three with C-shaped C-PSW/CF walls (15-story, 18-story, and 22-story, shown as Type II in Fig. 1). These walls were designed by Agrawal et al. (2020) and the structural details were chosen to be a reasonable representation of low-rise and mid-rise buildings. Moreover, C-PSW/CF walls were designed according to the requirements of AISC 341-16 (AISC 2016), Section H7, but with square closure end plates instead of round boundary elements.

Because the C-walls are being bent about their strong axis, the definition of flange and webs is reversed from what was presented earlier when considering C-walls bent about their weak axis. This is to be consistent with the common usage, whereby flanges are typically under (mostly) uniform stresses for a given applied moment. In the design procedure, initial parameters such as load requirements, building floor plan, and seismic parameters were chosen with the help of practicing engineers and a peer review panel. Some of the parameters are:

- Floor dimensions are [80 ft (24,384 mm) + X ft] × [180 ft (54,864 mm) + X ft], where X is the wall dimension;
- The height of the first floor is 17 ft (5,182 mm) but that of the remaining floors is 14 ft (4,267 mm);
- The floor load is 120 psf (0.83 MPa);
- An importance factor, I_e, of 1.0 was used with Risk Category II; and
- The seismic response modification factor, R, deflection amplification factor, C_d, and overstrength factor, Ω_o, are 6.5, 5.5, and 2.5, respectively.

More details about the design procedure can be found in Agrawal et al. (2020). For the current study, the archetypes listed in Tables 1 and 2 were used.

Table 1. Planar wall archetypes

Case	No. of stories	Wall thickness, t_{sc} (in.)	Wall length, L_{wall} (ft)	Plate thickness, t_p[a] (in.)	Height (ft)
1	3	12	15	4/16	45
2	6	16	25	5/16	87
3	9	24	30	7/16	129
4	12	32	35	8/16	171

Note: 1 in. = 25.4 mm; and 1 ft = 0.305 m.
[a]Same thickness used along building height.

Table 2. C-shaped wall archetypes

Case	No. of stories	Web depth, h_w (ft)	Flange length, h_f or L_{wall} (ft)	Web thickness, $t_{sc,w}$ (in.)	Flange thickness, $t_{sc,f}$ (in.)	Plate thickness, t_p[a] (in.)	Height (ft)
5	15	30	11	22	22	8/16	213
6	18	40	10	18	18	8/16	255
7	22	40	11	28	32	9/16	311

Note: 1 in. = 25.4 mm; and 1 ft = 0.305 m.
[a]Same thickness used along building height.

Nonlinear Models

Figs. 2(a and b) show two-dimensional OpenSees nonlinear models for the collapse simulation of the planar C–PSW/CF and C-shaped C-PSW/CF archetypes. The *Reinforcing Steel* (McKenna et al. (2016) and *Concrete02* material models in the OpenSees library were used for the steel and concrete fibers in the cross-sections of the planar and C-shaped walls. This steel hysteretic model was used to model the plates because it had the ability to capture both inelastic buckling and failure due to low-cycle fatigue life—the two main factors that ultimately drive strength degradation of the wall's hysteretic behavior. The same steel grade was used for web and flanges, namely, ASTM A572 Gr 50. Therefore, the same buckling and low-fatigue parameters were assigned to the reinforcing steel material used for the flanges and web. Also, the concrete confinement model by Susantha et al. (2001) was used to determine the concrete strength and ductility at the ends of the cross section over a length equal to half the width of the cross section, while the rest of the concrete cross section was assigned a concrete model having unconfined concrete strength but the same ductility as that of the confined concrete. Tables 3 and 4 show the steel and concrete inputs for the *Reinforcing Steel* and *Concrete02* material models. Displacements based nonlinear beam-column elements were used to connect the cross-sections. Calibration of planar wall

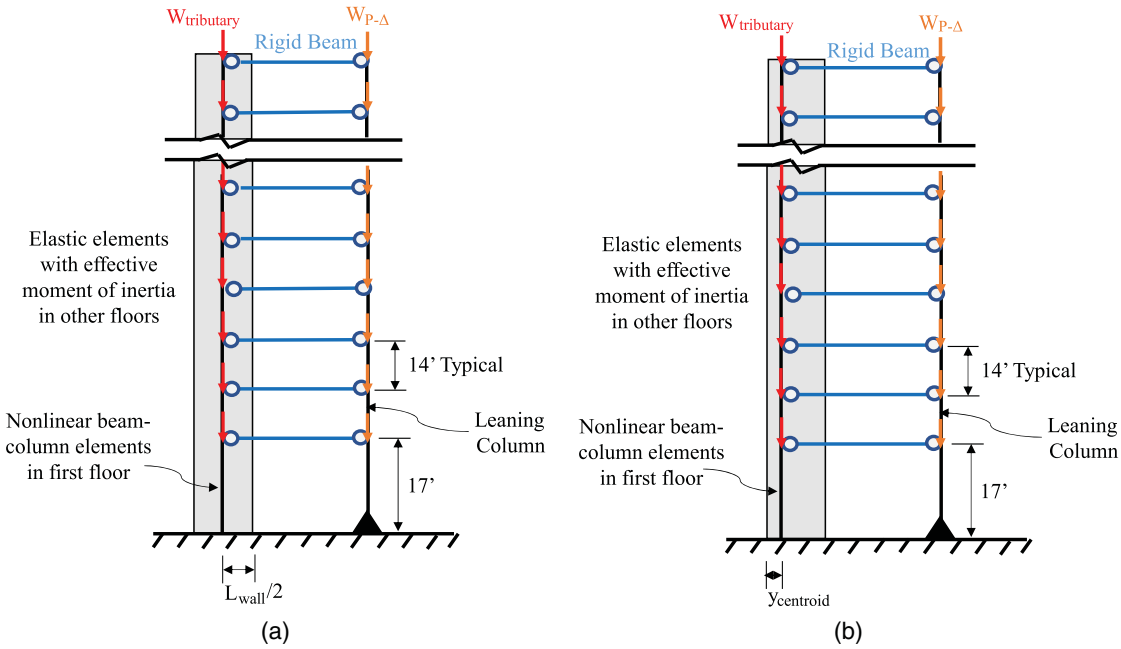

Fig. 2. Representation of OpenSees models of (a) planar wall archetypes; and (b) C-shaped wall archetypes. (Note: 1 ft = 0.305 m.)

Table 3. Steel inputs for planar and C-shaped C-PSW/CF walls

Parameters	Planar walls	C-shaped walls
f_y (ksi)	50.0	50.0
E_s (ksi)	29,000	29,000
ε_y	0.0017	0.0017
f_u (ksi)	61.0	57.0
E_{sh} (ksi)	$0.0543 \times E_s$	$0.01 \times E_s$
ε_{sh}	0.0018	0.0018
ε_u	0.15	0.15
l_{SR}	20.8	25.6
β	1.0	1.0
r	0.4	0.9
γ	1.0	1.0
C_f	0.21	0.21
α	0.515	0.575
C_d	0.3	0.4
R1,R2.R3	0.333; 18.0; 4.0	0.333; 18.0; 4.0
a1, limit	4.3; 0.01	4.3; 0.01

Note: 1 ksi = 6.89 MPa.

models was done based on the tests conducted by Shafaei et al. (2021) and calibration of C-shaped wall models was done based on the tests conducted by Kenarangi et al. (2021). Based on the observed behavior from planar and C-and T- shaped wall tests by Shafaei et al. (2021), Kenarangi et al. (2021), and Kizilarslan and Bruneau (2023), fiber element modeling was deemed adequate for the current purpose and good agreement was achieved between test and model results. Note that C-SPW/CF have been reported to dominantly behave in flexure for aspect ratios as low as 1.5 because of their large shear strength and stiffness (Kurt et al. 2015). Note also that, although not presented here, some analyses with force-based nonlinear elements were also conducted, but this element was found to be computational expensive and not preferred due to occasional lack of convergence in nonlinear time-history analyses. Instead, displacement-based elements with more elements at the base were used in the plastic hinge zone to get more accuracy (Neuenhofer and Filippou 1997); details can be found in Kizilarslan et al. (2021a) and Kizilarslan (2021). However, even though the non-linear models and low-cycle fatigue parameters for the C-shaped walls were calibrated for flexure about their weak axis, here the same models based on the same calibrations were used for flexure about the strong. For walls, based on findings from prior studies on coupled walls that demonstrated this to be appropriate (Bruneau et al. 2019; Kizilarslan et al. 2021b), the nonlinear beam column elements were only assigned up to the first floor and the rest of the floors were modeled using elastic beam-column elements having effective stiffness per AISC Equation I2-12. Leaning columns were also modeled to include the P–Δ effects in each given story due to gravity loads. [Note that, due to changes in floor plans, each archetype has different gravity loads (specifically, 1,200 kips, 1,292 kips, 1,386 kips, 1,484 kips, 1,386 kips, 1,512 kips, and 1,512 kips (5,338 kN, 5,747 kN, 6,165 kN, 6,601 kN, 6,165 kN, 6,726 kN, and 6,726 kN) for Cases 1, 2, 3, 4, 5, 6, and 7, respectively.] Elastic beam-column elements were used to model leaning columns. Because there is no definitive information on the number of leaning columns in the archetype design, the values of moment of inertia and cross section area

Table 4. Concrete inputs for planar and C-shaped C-PSW/CF walls

Specimens	f_{PC} (ksi) (unconf./confined)	E_C (ksi)	$\varepsilon_{co} \times 10^{-3}$ (unconf./confined)	f_{CU} (ksi) (unconf./confined)	ε_{cu}	Lambda	Z (ksi)	α
Planar walls	6.0/6.78	4,415	2.72/3.071	5.08/5.74	0.04	0.7	25	0.883
C-shaped walls	6.0/6.78	4,415	2.72/3.071	5.08/5.74	0.04	0.1	20	0.883

Note: 1 ksi = 6.89 MPa; and Unconf. = unconfined.

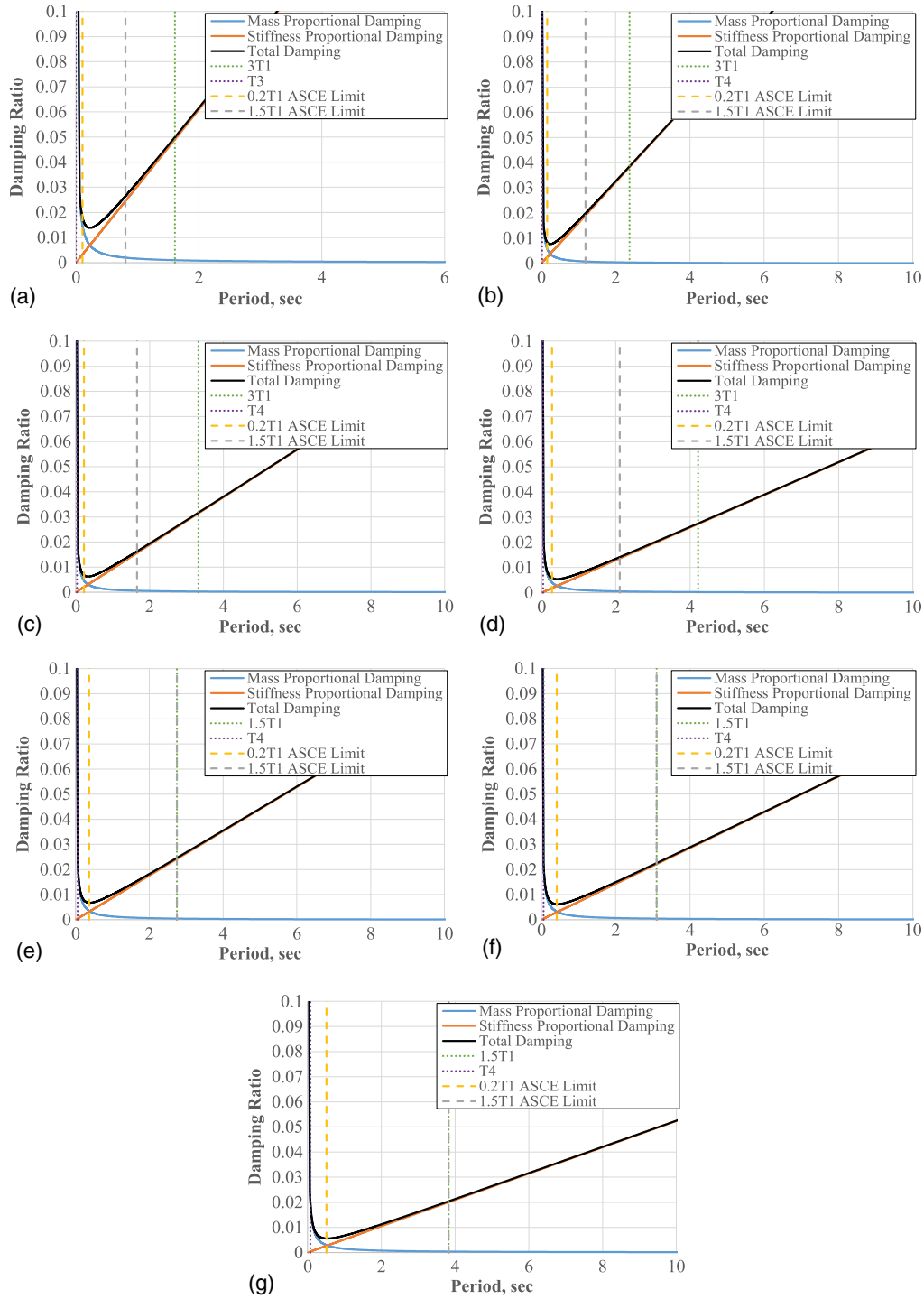

Fig. 3. Damping curves for: (a) Case 1; (b) Case 2; (c) Case 3; (d) Case 4; (e) Case 5; (f) Case 6; and (g) Case 7.

of the elastic beam-column elements were arbitrarily chosen to provide insignificant flexural stiffness. Tributary loads coming to the C-PSW/CF walls [180 kips, 189 kips, 198 kips, and 207 kips (801 kN, 841 kN, 881 kN, and 921 kN) per floor for the planar walls in Cases 1, 2, 3, and 4; and 198 kips, 216 kips, and 216 kips (881 kN, 961 kN, and 961 kN) for the C-shaped walls in Cases 5, 6, and 7] were applied at each floor. Rigid beams were used to link the leaning column to the C-PSW/CF wall at every floor. (These rigid beams were modeled using truss elements with an arbitrarily large cross section.) Seismic masses were assigned to the C-PSW/CF walls at every story.

Table 5. Damping details for the archetypes

Case	First period (s)	Anchored periods (s)	Damping ratio (%)	Damping ratio at first period (%)
1	0.54	1.61-0.032 (3T1-T3)	5.00	1.93
2	0.79	2.38-0.024 (3T1-T4)	3.86	1.39
3	1.107	3.32-0.033 (3T1-T4)	3.17	1.14
4	1.405	4.22-0.042 (3T1-T4)	2.75	0.99
5	1.83	2.75-0.054 (1.5T1-T4)	2.47	1.68
6	2.07	3.1-0.061 (1.5T1-T4)	2.25	1.54
7	2.55	3.83-0.075 (1.5T1-T4)	2.04	1.4

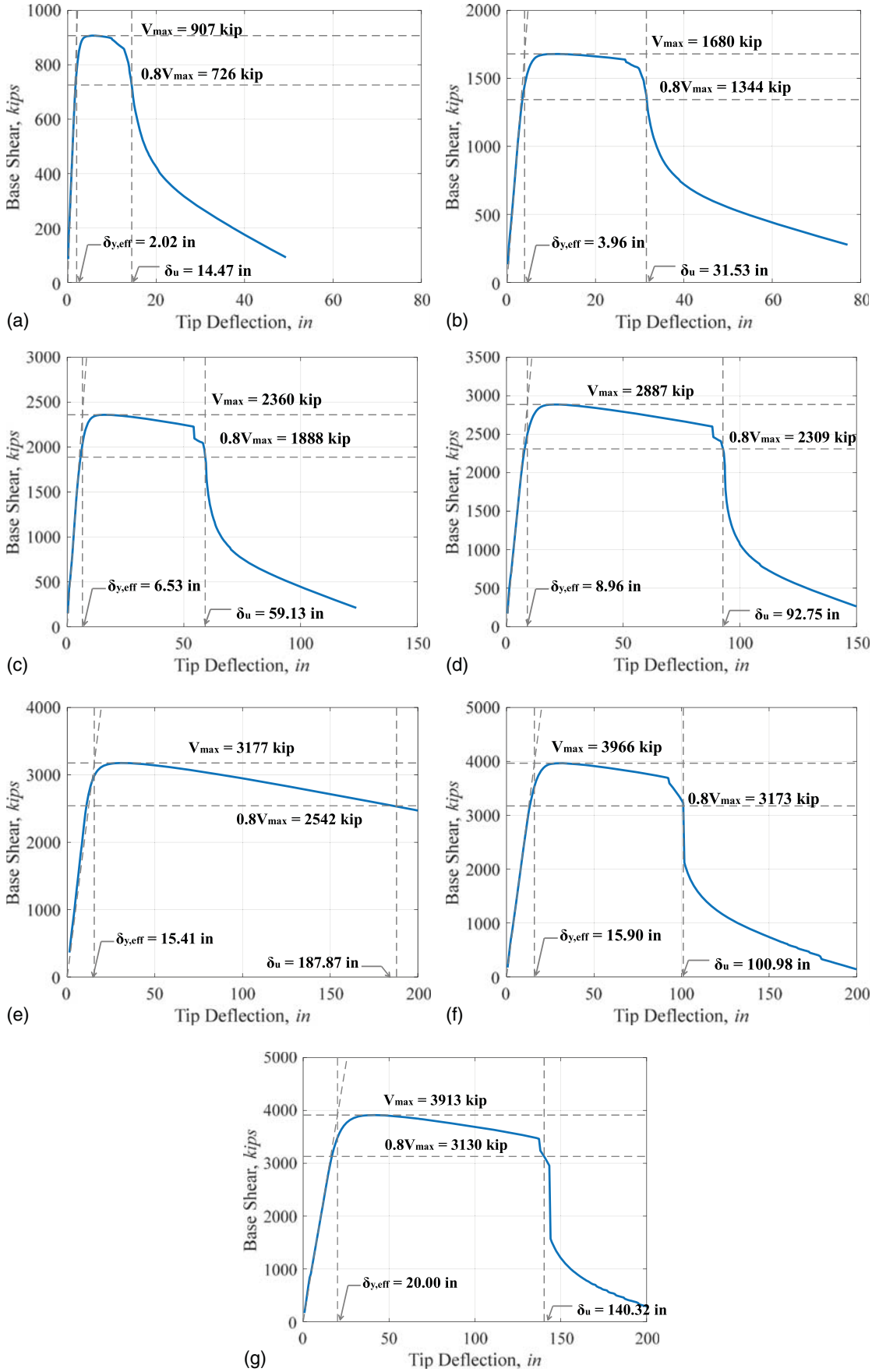

Fig. 4. Pushover curves for: (a) Case 1; (b) Case 2; (c) Case 3; (d) Case 4; (e) Case 5; (f) Case 6; and (g) Case 7. (Note: 1 in. = 25.4 mm; 1 kip = 4.45 kN.)

In the nonlinear time history analyses of the archetypes, Rayleigh damping was used. In all of the archetypes, 90% of the total mass participation factor was reached when the first four modes of vibration were considered (or the first three modes of vibration for the 3-story archetype). In these analyses, the damping ratio was reduced to a value based on the height of the structure, in accordance with the following equation from PEER TBI: Equivalent Viscous Damping (PEER 2010):

$$\xi_{critical} = \frac{0.36}{\sqrt{H}} \quad (1)$$

where H is the height of the structure in feet.

After further studying the behavior of these lateral loading resisting systems, it was observed that the composite walls were vibrating individually at a much larger period of vibration after buckling or fracture develops, and that that response eventually transformed into a rocking behavior after excessive damage in the plastic hinge region. As a result, the period of the system elongates significantly as it progresses towards that stage of severe damage. In order to prevent overdamping of the structural system when it shifts to those higher periods of vibration, it was decided to perform these analyses with a reduced damping ratio anchored at three times the first period, and at the fourth period of vibration for planar walls; and one-and-a-half times the first period and at the fourth period of vibration for the C-shaped walls (Fig. 3). These multipliers of the first period were determined from observation of the results from nonlinear analyses of each archetype. Table 5 presents the details of the damping ratio of each archetype and the periods used to define the Rayleigh damping for this study.

Nonlinear Analyses

Nonlinear Pushover Analysis

Nonlinear pushover analysis was also conducted, in compliance with the approach prescribed by the FEMA P695 methodology, in order to estimate the overstrength (Ω_o) and period-based ductility (μ_T) factors for all archetypes. The results of the pushover analysis for the archetypes are shown in Fig. 4. The overstrength (Ω_o) factor was found by dividing the maximum base shear obtained from the static pushover curve by the base shear for which the archetypes were designed, as shown in Table 6. The period-based ductility (μ_T) factor was determined by dividing the effective yield displacement by the ultimate top floor displacements. The displacement corresponding to the intersection of a line tangent to the initial slope of the resulting pushover curve and a horizontal line set at the level of the maximum base shear obtained from this nonlinear pushover analysis, $V_{\max}$, was considered as the effective yield displacement ($\delta_{y,\text{eff}}$), and the displacement obtained at $0.8\,V_{\max}$ on the descending branch (i.e., post-peak) of the pushover curve was taken for the ultimate top floor displacement (δ_u). The nonlinear pushover results of all archetypes are presented in Fig. 4.

The strength degradation in the pushover curves of the planar walls (Cases 1 to 4) becomes rather sudden after a plateau of inelastic deformation. The curves for the C-shaped walls follow a similar trend, except that the drop in strength is very steep in Cases 6 and 7. In these last two cases, a particularly sudden fracture was observed. In all cases, the decrease in strength is first due to buckling. Then, at the point of rapid and sudden drop in strength, this is due to fracture, with the most abrupt drops due to fracture of the full web. Recall that

Table 6. Pushover analysis results of archetypes

	Archetypes with planar walls				Archetypes with C-shaped walls		
Parameters	Case 1	Case 2	Case 3	Case 4	Case 5	Case 6	Case 7
$V_{\max}$, kips	907	1,680	2,360	2,887	3,177	3,966	3,913
V_{design}, kips	553	897	1,074	1,160	1,230	1,470	1,485
$\Omega_o = V_{\max}/V_{\text{design}}$	1.64	1.87	2.20	2.49	2.58	2.70	2.64
$\delta_{y,\text{eff}}$, in.	2.02	3.96	6.53	8.96	15.41	15.90	20.00
δ_u, in.	14.47	31.53	59.13	92.75	187.87	100.98	140.32
$\mu_T = \delta_u/\delta_{y,\text{eff}}$	7.16	7.96	9.06	10.35	12.19	6.35	7.02

Note: 1 in. = 25.4 mm; and 1 kip = 4.45 kN.

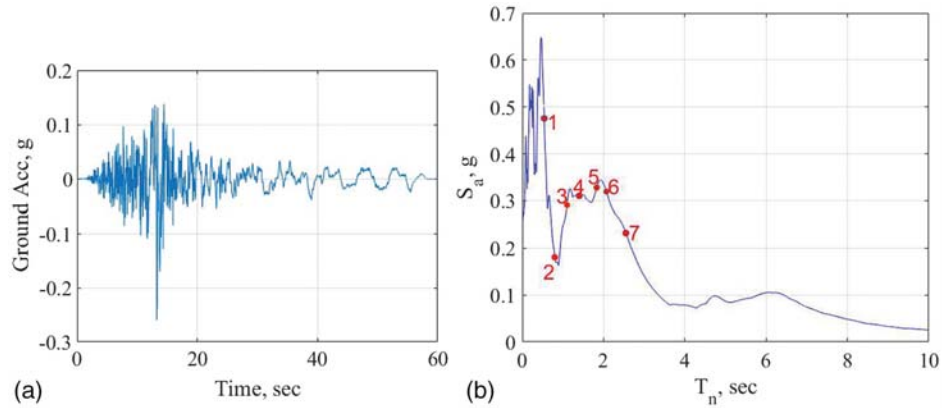

Fig. 5. Ground acceleration of (a) BICC090 earthquake; and (b) acceleration spectrum with periods of archetypes.

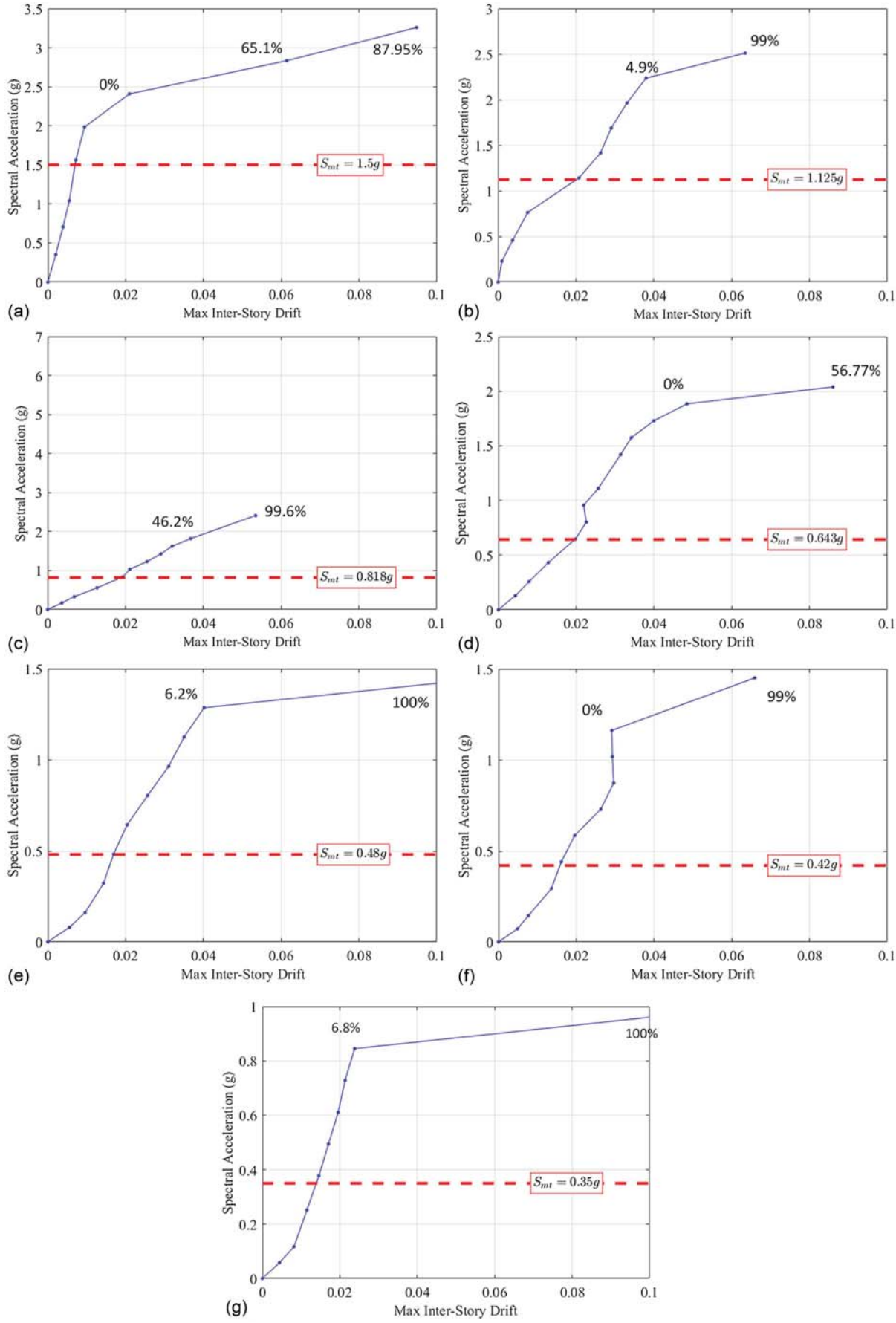

Fig. 6. Incremental dynamic analysis curves of (a) Case 1; (b) Case 2; (c) Case 3; (d) Case 4; (e) Case 5; (f) Case 6; and (g) Case 7 for BICC090 earthquake with fracture percentages.

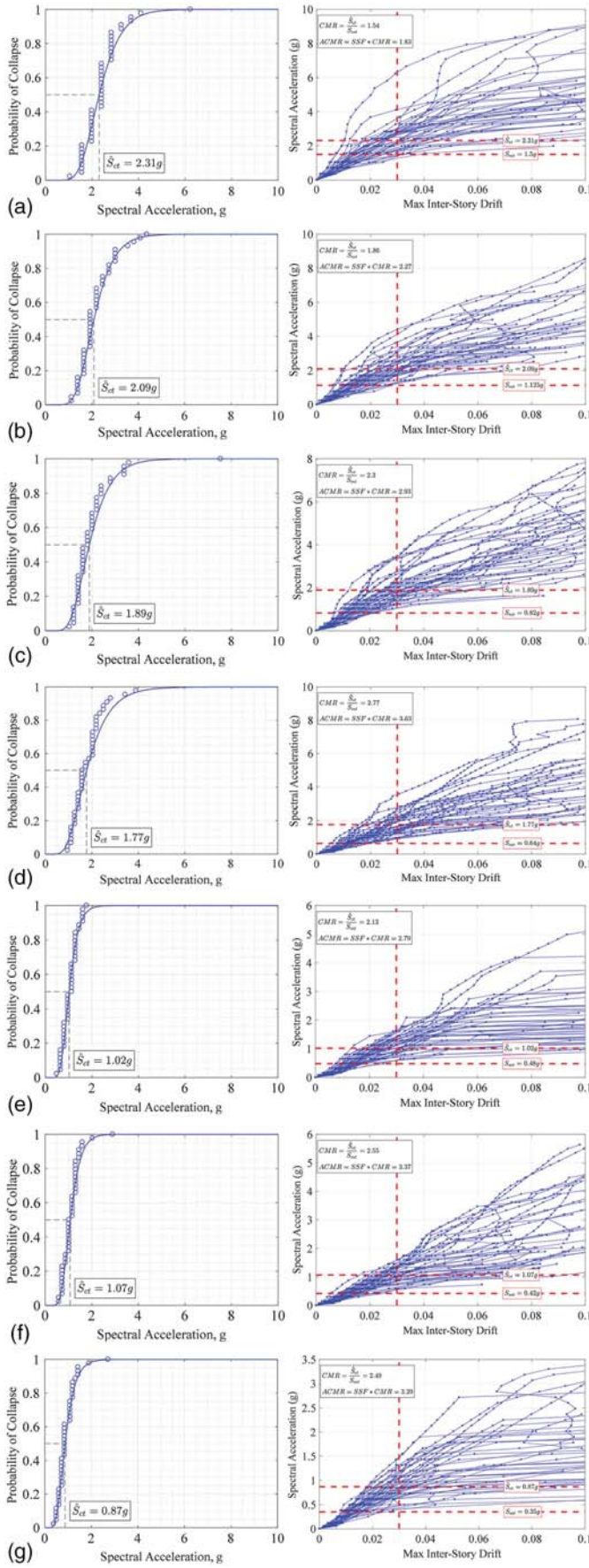

Fig. 7. Fragility and IDA curves at 3% maximum interstory drift for (a) Case 1; (b) Case 2; (c) Case 3; (d) Case 4; (e) Case 5; (f) Case 6; and (g) Case 7.

these archetypes were modelled for bending about their strong axis, so once the flange of the C-shaped walls fractures, most of the wall flexural strength is lost.

Incremental Dynamic Analysis of Archetypes

IDA consists of a series of successive time history analyses performed for a given structural model, for which the intensity of the specified ground motions is gradually scaled up from low to high magnitude until collapse is observed in the structure. In this research project that considers the 44 far-field ground motions specified in FEMA P695, the IDA started with an analysis using half of the actual unscaled recorded ground motions, followed by one using the actual unscaled record itself. The subsequent increments for all ground motions were scaled such that the median spectral acceleration of the 44 ground motions (at the fundamental period of a given archetype being analyzed) matched that at the design basis earthquake (DBE) and at the maximum considered earthquake (MCE) spectral acceleration levels. From there, each motion was gradually scaled up in steps equal to 0.6 and to 1.0 times the MCE level (i.e., $0.6\,S_{a\text{–MCE}}$, and $1.0\,S_{a\text{–MCE}}$) for planar and C-shaped archetypes, respectively, up to the intensity that caused structural collapse for each individual ground motion.

In a typical IDA curve, when the intensity measure (IM) vs damage measure (DM) curves become a nearly flat line upon increasing values of IM, it is an indication of structural collapse. However, in most cases, for the types of structure considered here, collapse by this definition was often observed to occur at extreme drifts of nearly 10% (or even 15% in some cases). As such, other considerations must be considered to define "collapse" from a practical perspective.

Past experiments on individual C-SPW/CF walls tested them up to 4% and 5% drift (Kenarangi et al. 2021; Kizilarslan and Bruneau 2023; Shafaei et al. 2021). It was reported in these tests that the initiation of local buckling started as soon as at 1.5% drift, but that flexural strength degradation only occurred with fracture initiation at typically larger drifts. The IDA analysis results revealed that collapse typically occurred at drifts as large as 10%, which was deemed to be an excessive reference point for this study. Because the hysteretic energy dissipation mechanism in single uncoupled walls during earthquake excitation only occurs at their base, it was arbitrarily decided to define collapse (i.e., to limit the damage measure, DM) at 3% maximum interstory drift. This was not a requirement of the FEMA P695 procedure, but rather a judgment call to obtain more conservative results. Moreover, to support this conclusion, a study was performed to determine at which drift the archetypes experienced severe damage. It was believed that using an earthquake with large pulses would more severely challenge the numerical calculations. For this purpose, one of the most severe ground motions among the 44 that the FEMA P695 procedure provides was used, namely the N-S component of the Superstition Hills (BICC090) earthquake [Fig. 5(a)]. This record was selected because it exhibits multiple pulses and is of significant duration. For example, between the times of 30.78 and 33.39 s [Fig. 5(a)],

Table 7. IDA results of archetypes at 3% drift

	Archetypes with planar walls				Archetypes with C-shaped walls		
Parameter	Case 1	Case 2	Case 3	Case 4	Case 5	Case 6	Case 7
S_{CT}, g	2.31	2.09	1.89	1.77	1.02	1.07	0.87
S_{MT}, g	1.5	1.125	0.82	0.64	0.48	0.42	0.35
CMR $= S_{CT}/S_{MT}$	1.54	1.86	2.3	2.77	2.13	2.55	2.49

Note: Units = kips, in., s, g.

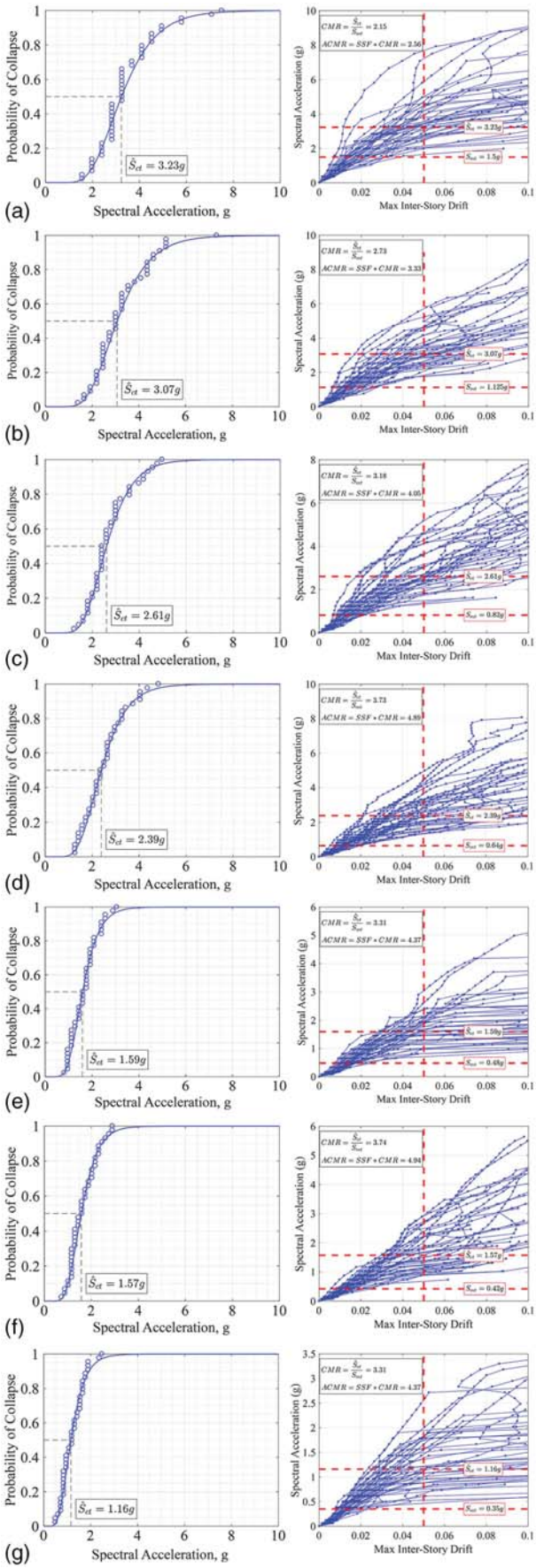

Fig. 8. Fragility and IDA curves at 5% maximum interstory drift for (a) Case 1; (b) Case 2; (c) Case 3; (d) Case 4; (e) Case 5; (f) Case 6; and (g) Case 7.

the area under the ground acceleration is large, indicating a large velocity pulse. This ground motion was also selected because the shape of its response spectra is such that the spectral acceleration demands at the periods of the archetypes are large and remains large at adjacent larger periods [and slightly larger for that matter, as seen in Fig. 5(b)], which will keep seismic demand intense as the archetypes undergo nonlinear inelastic response and their periods elongate, thus making the archetypes more prone to collapse. Figs. 6(a–g) show the IDA of the archetypes for this BICC090 earthquake and the percent of fracture at the base of the wall that developed at each intensity increment close to collapse. In other words, in these figures the percentage values shown express the percentage of the wall cross section that is fractured by the end of the earthquake excitation. The results indicate that, once fracture initiated, at the next increase in ground motion intensity that was considered, the increase in cross-section fracture was substantial. For example, in Fig. 6(a), while there was no fracture when the earthquake was scaled to produce a 2.4 g spectral acceleration, 65% and 88% of the cross section was fractured when analysis was conducted at the end of the next scaled two intensity levels (2.8 g and 3.4 g). However, less sudden increases from one intensity to the other might have been noticed if the scaling steps of the IDA had been smaller. Also, in Fig. 6, most of the archetypes are observed to have experienced severe damage (buckling and fracture) at 5% maximum interstory drift, which is the drift that was chosen in previous similar FEMA P-695 studies for coupled composite plate shear walls (CC-PSW/CF). However, because all the archetypes of uncoupled walls must resist all the seismic demand without the added benefit of ductile coupling beams, to be more conservative, the collapse margin ratio (CMR) is calculated here based on the response values obtained at 3% drift for each archetype. In other words, reaching a drift of 3% is defined as collapse for the purposes of this FEMA P-695 study.

Fig. 7 present the IDA results obtained for all planar and C-shaped archetypes considered and their corresponding fragility curves developed based on the spectral accelerations at the point closest to 3% maximum interstory drift. The fragility curves were directly constructed from the IDA results; as such, they represent the proportion (normalized from 0 to 1) of the cases that reached specific spectral accelerations at the 3% interstory drift level, although, practically, only the median value from this data is needed for the FEMA P695 procedure. For each archetype, the median collapse spectral acceleration intensity at 3% maximum interstory drift, $\hat{S}_{CT}$, was taken from its corresponding collapse fragility curve as the spectral acceleration intensity that corresponded to a 50% probability of collapse at 3% maximum interstory drift. These curves were obtained by fitting a lognormal distribution through the collapse data points. The median collapse spectral acceleration intensity, $\hat{S}_{CT}$, and the median spectral acceleration, S_{MT}, are also compiled in Table 7. From these IDA results, the CMR was calculated as the ratio between $\hat{S}_{CT}$ and S_{MT}. For comparison with the results obtained by defining collapse at 3% drift, $\hat{S}_{CT}$ was also calculated for collapse

Table 8. IDA results of archetypes at 5% drift

	Archetypes with planar walls				Archetypes with C-shaped walls		
Parameter	Case 1	Case 2	Case 3	Case 4	Case 5	Case 6	Case 7
S_{CT}, g	3.23	3.07	2.61	2.39	1.59	1.57	1.16
S_{MT}, g	1.5	1.125	0.82	0.64	0.48	0.42	0.35
CMR = S_{CT}/S_{MT}	2.15	2.73	3.18	3.73	4.37	3.74	3.31

Note: Units = kips, in., s, g.

defined as a 5% maximum interstory drift, similarly to what had been done in the previous study on coupled walls. The corresponding results from 5% maximum interstory drift are shown in Fig. 8 and Table 8.

Collapse Performance Evaluation

Tables 9 and 10 compare collapse performance evaluations for planar and C-shaped archetypes, by summarizing design information, nonlinear static and dynamic analyses results, and evaluation of the seismic performance factors used for the original design. The initial step of the performance evaluation is to adjust the CMR value obtained from the IDA to take into account the frequency content of the selected ground motion records (i.e., the effect of spectral shape). The spectral shape factor (SSF) values that are used to modify the CMR to the adjusted collapse margin ratio (ACMR) are a function of the archetype fundamental period, the applicable seismic design category (SDC), and period-based ductility (μ_T) attained from nonlinear pushover analysis. The fundamental period (T) of the archetypes was used instead of the maximum period for which the archetypes were designed. (Note that this does not make a significant difference in the results.) The period-based ductility (μ_T) was conservatively taken as 3 for all archetypes, based on observed behavior in experimentally obtained cyclic hysteretic curves, even though the nonlinear pushover analysis of archetypes proved that the ductility is more than 3 for all archetypes. The values of SSF are obtained from Tables 7-1a and 7-1b (depending on SDC) in the FEMA P695 document for both archetypes. Accordingly, the ACMR are obtained by multiplying the CMR by the SSF value. These values are compared to acceptable ACMR values to verify if the initial R factor used to design these archetypes satisfies the FEMA P695 requirements.

As such, total system collapse uncertainty (β_{TOT}) is required in order to calculate an acceptable ACMR value. The value of β_{TOT} is obtained by combining uncertainty factors related to record-to-record (β_{RTR}), design requirements (β_{DR}), test data (β_{TD}), and nonlinear modeling (β_{MDL}). For the selected ground motions used in the FEMA P695 methodology, a constant value of β_{RTR} equal to 0.4 is used, given that period-based ductility is larger than or equal to 3 ($\mu_T \geq 3$). With respect to the other three uncertainty factors (β_{DR}, β_{TD}, and β_{MDL}), these values were taken as equal to 0.2, corresponding to the "good" rating (i.e., β_{DR}, β_{TD}, and $\beta_{\text{MDL}} = 0.2$). The corresponding total system uncertainty calculated using Eq. (2) is 0.529. The acceptable ACMR for 10% and 20% collapse probability under MCE ground motions (i.e., $\text{ACMR}_{10\%}$ and $\text{ACMR}_{20\%}$) for β_{TOT} of 0.529 are specified to be 1.96 and 1.56 in Table 9-7 of the FEMA P695 document, respectively

$$\beta_{total} = \sqrt{\beta_{RTR}^2 + \beta_{DR}^2 + \beta_{TD}^2 + \beta_{MDL}^2} \tag{2}$$

The FEMA P695 methodology specifies that $\text{ACMR}_{10\%}$ and $\text{ACMR}_{20\%}$ are the acceptable threshold values to evaluate performance of individual archetype and average performance of several archetypes in one performance group, respectively. Hence, here all

Table 9. Summary of ATC-63 methodology on archetypes with planar walls at 3% maximum interstory drift: Case 1, 2, 3, and, 4

Parameter	Case 1	Case 2	Case 3	Case 4	Note and reference
			1. Design stage		
R	6.5	6.5	6.5	6.5	ASCE 7-10 (Table 12.2-1)
V_{design}	553	897	1,074	1,160	From ELF method
			2. Nonlinear static (pushover) analysis		
V_{max}	907	1,680	2,360	2,887	—
$\Omega_o = V_{\text{max}}/V_{\text{design}}$	1.64	1.87	2.20	2.49	—
$\delta_{y,\text{eff}}$	2.02	3.96	6.53	8.96	—
δ_u	14.47	31.53	59.13	92.75	
$\mu_T = \delta_u/\delta_{y,\text{eff}}$	7.16	7.96	9.06	10.35	—
			3. IDA		
S_{CT}	2.31	2.09	1.89	1.77	—
S_{MT}	1.5	1.125	0.82	0.64	
$\text{CMR} = S_{\text{CT}}/S_{\text{MT}}$	1.54	1.86	2.3	2.77	—
			4. Performance evaluation		
T	0.54	0.80	1.11	1.4	From OpenSees
SDC	D_{max}	D_{max}	D_{max}	D_{max}	FEMA P695 (Table 5-1)
SSF (T, μ_T, SDC)	1.19	1.22	1.28	1.31	FEMA P695 (Table 7-1)
ACMR	1.83	2.27	2.94	3.63	—
β_{RTR}	0.4	0.4	0.4	0.4	"Good" rating
β_{DR}, β_{TD}, β_{MDL}	0.2	0.2	0.2	0.2	
β_{tot}	0.529	0.529	0.529	0.529	—
$\text{ACMR}_{20\%}$ (β_{tot})	1.56	1.56	1.56	1.56	FEMA P695 (Table 7-3)
$\text{ACMR}_{10\%}$ (β_{tot})	1.96	1.96	1.96	1.96	
Status_{i}	Pass	Pass	Pass	Pass	Pass if $\text{ACMR}_{20\%} < \text{AMCR}$
AMCR_{ave}			2.67		Average in a performance group
$\text{Status}_{\text{PG}}$			Pass		Pass if $\text{ACMR}_{10\%} < \text{AMCR}_{\text{ave}}$
			5. Final results		
R	6.5	6.5	6.5	6.5	—
Ω_o	1.64	1.87	2.20	2.49	—
μ_T	7.16	7.96	9.06	10.35	—
C_d	5.5	5.5	5.5	5.5	—

Note: Units = kips, in., s, g.

Table 10. Summary of ATC-63 methodology on archetypes with C-shaped walls at 3% maximum interstory drift: 7

Parameter	Case 5	Case 6	Case 7	Note and reference
		1. Design stage		
R	6.5	6.5	6.5	ASCE 7-10 (Table 12.2-1)
V_{design}	1,230	1,470	1,485	From ELF method
		2. Nonlinear static (pushover) analysis		
$V_{\max}$	3,177	3,966	3,913	—
$\Omega_o = V_{\max}/V_{\text{design}}$	2.58	2.70	2.64	—
$\delta_{y,\text{eff}}$	15.41	15.90	20.00	—
δ_u	187.87	100.98	140.32	—
$\mu_T = \delta_u/\delta_{y,\text{eff}}$	12.19	6.35	7.02	—
		3. IDA		
S_{CT}	1.02	1.07	0.87	—
S_{MT}	0.48	0.42	0.35	
$\text{CMR} = S_{\text{CT}}/S_{\text{MT}}$	2.13	2.55	2.49	—
		4. Performance evaluation		
T	1.83	2.07	2.55	From OpenSees
SDC	$D_{\max}$	$D_{\max}$	$D_{\max}$	FEMA P695 (Table 5-1)
$\text{SSF}(T, \mu_T, \text{SDC})$	1.32	1.32	1.32	FEMA P695 (Table 7-1)
ACMR	2.81	3.37	3.29	—
β_{RTR}	0.4	0.4	0.4	"Good" rating
β_{DR}, β_{TD}, β_{MDL}	0.2	0.2	0.2	
β_{tot}	0.529	0.529	0.529	—
$\text{ACMR}_{20\%}$ (β_{tot})	1.56	1.56	1.56	FEMA P695 (Table 7-3)
$\text{ACMR}_{10\%}$ (β_{tot})	1.96	1.96	1.96	—
Status_i	Pass	Pass	Pass	Pass if $\text{ACMR}_{20\%} < \text{AMCR}$
AMCR_{ave}		3.16		Average in PG
$\text{Status}_{\text{PG}}$		Pass		Pass if $\text{ACMR}_{10\%} < \text{AMCR}_{\text{ave}}$
		5. Final results		
R	6.5	6.5	6.5	—
Ω_o	2.58	2.70	2.64	—
μ_T	12.19	6.35	7.02	—
C_d	5.5	5.5	5.5	—

Note: Units = kips, in., s, g.

Table 11. Summary of ATC-63 methodology on archetypes with planar walls at 5% maximum interstory drift: Case 1, 2, 3, and, 4

Parameter	Case 1	Case 2	Case 3	Case 4	Note and reference
			1. Design stage		
R	6.5	6.5	6.5	6.5	ASCE 7-10 (Table 12.2-1)
V_{design}	553	897	1,074	1,160	From ELF method
			2. Nonlinear static (pushover) analysis		
$V_{\max}$	907	1,680	2,360	2,887	—
$\Omega_o = V_{\max}/V_{\text{design}}$	1.64	1.87	2.20	2.49	—
$\delta_{y,\text{eff}}$	2.02	3.96	6.53	8.96	—
δ_u	14.47	31.53	59.13	92.75	
$\mu_T = \delta_u/\delta_{y,\text{eff}}$	7.16	7.96	9.06	10.35	—
			3. IDA		
S_{CT}	3.23	3.07	2.61	2.39	—
S_{MT}	1.5	1.125	0.82	0.64	
$\text{CMR} = S_{\text{CT}}/S_{\text{MT}}$	2.15	2.73	3.18	3.73	—
			4. Performance evaluation		
T	0.54	0.80	1.11	1.4	From OpenSees
SDC	$D_{\max}$	$D_{\max}$	$D_{\max}$	$D_{\max}$	FEMA P695 (Table 5-1)
$\text{SSF}(T, \mu_T, \text{SDC})$	1.19	1.22	1.28	1.31	FEMA P695 (Table 7-1)
ACMR	2.56	3.33	4.05	4.89	—
β_{RTR}	0.4	0.4	0.4	0.4	"Good" rating
β_{DR}, β_{TD}, β_{MDL}	0.2	0.2	0.2	0.2	
β_{tot}	0.529	0.529	0.529	0.529	
$\text{ACMR}_{20\%}$ (β_{tot})	1.56	1.56	1.56	1.56	FEMA P695 (Table 7-3)
$\text{ACMR}_{10\%}$ (β_{tot})	1.96	1.96	1.96	1.96	
Status_i	Pass	Pass	Pass	Pass	Pass if $\text{ACMR}_{20\%} < \text{AMCR}$
AMCR_{ave}			3.71		Average in a performance group
$\text{Status}_{\text{PG}}$			Pass		Pass if $\text{ACMR}_{10\%} < \text{AMCR}_{\text{ave}}$

Table 11. (*Continued.*)

Parameter	Case 1	Case 2	Case 3	Case 4	Note and reference
			5. Final results		
R	6.5	6.5	6.5	6.5	—
Ω_o	1.64	1.87	2.20	2.49	—
μ_T	7.16	7.96	9.06	10.35	—
C_d	5.5	5.5	5.5	5.5	—

Note: Units = kips, in., s, g.

Table 12. Summary of ATC-63 methodology on archetypes with C-shaped walls at 5% maximum interstory drift: Case 5, 6, and, 7

Parameter	Case 5	Case 6	Case 7	Note and reference
		1. Design stage		
R	6.5	6.5	6.5	ASCE 7-10 (Table 12.2-1)
V_{design}	1,230	1,470	1,485	From ELF method
		2. Nonlinear static (pushover) analysis		
$V_{\max}$	3,177	3,966	3,913	—
$\Omega_o = V_{\max}/V_{\text{design}}$	2.58	2.70	2.64	—
$\delta_{y,\text{eff}}$	15.41	15.90	20.00	—
δ_u	187.87	100.98	140.32	—
$\mu_T = \delta_u/\delta_{y,\text{eff}}$	12.19	6.35	7.02	—
		3. IDA		
S_{CT}	1.59	1.57	1.16	—
S_{MT}	0.48	0.42	0.35	
$\text{CMR} = S_{\text{CT}}/S_{\text{MT}}$	4.37	3.74	3.31	—
		4. Performance evaluation		
T	1.83	2.07	2.55	From OpenSees
SDC	$D_{\max}$	$D_{\max}$	$D_{\max}$	FEMA P695 (Table 5-1)
SSF(T, μ_T, SDC)	1.32	1.32	1.32	FEMA P695 (Table 7-1)
ACMR	4.37	4.94	4.37	—
β_{RTR}	0.4	0.4	0.4	"Good" rating
β_{DR}, β_{TD}, β_{MDL}	0.2	0.2	0.2	
β_{tot}	0.529	0.529	0.529	—
$\text{ACMR}_{20\%}$ (β_{tot})	1.56	1.56	1.56	FEMA P695 (Table 7-3)
$\text{ACMR}_{10\%}$ (β_{tot})	1.96	1.96	1.96	—
Status_{i}	Pass	Pass	Pass	Pass if $\text{ACMR}_{20\%} < \text{AMCR}$
AMCR_{ave}		4.56		Average in PG
$\text{Status}_{\text{PG}}$		Pass		Pass if $\text{ACMR}_{10\%} < \text{AMCR}_{\text{ave}}$
		5. Final results		
R	6.5	6.5	6.5	—
Ω_o	2.58	2.70	2.64	—
μ_T	12.19	6.35	7.02	—
C_d	5.5	5.5	5.5	—

Note: Units = kips, in., s, g.

archetypes satisfied the specified performance requirement. The results in Tables 9 and 10 show that for a β_{TOT} of 0.529 and a "good" rating, all archetypes are considerably above the $\text{ACMR}_{20\%}$ threshold. Likewise, the average of ACMR values in a performance group also passed the $\text{ACMR}_{10\%}$ threshold.

Note that the results using 5% maximum interstory drift are also presented in Tables 11 and 12. The results in that case more easily passed both threshold ACMR values. Also, in an average sense, the results are 28% and 31% larger for the planar and C-shaped archetypes, respectively, compared to the case where a 3% maximum interstory drift was considered as the response limit.

Summary and Conclusion

In this work, the seismic design factors for C-PSW/CF are verified by conducting a FEMA P695 study. A study was needed, as these factors, included in ASCE 7 since as far back as its 2000 edition, were chosen solely based on the seismic performance of similar structural systems and engineering judgment of the committee members.

For this study, four archetypes with planar walls (3-story, 6-story, 9-story, and 12-story) and three archetypes with C-shaped C-PSW/CF walls (15-story, 18-story, and 22-story) designed by others were chosen, as these provided a reasonable representation of low-rise and mid-rise buildings designed in compliance with the requirements of AISC 341-16, Section H7; however, square closure end plates instead of round boundary elements were used (Agrawal et al. 2020).

Two different DMs were chosen for this study: 3% and 5% maximum interstory drifts. The incremental dynamic analyses performed as part of this study showed that most of the archetypes experienced severe damage at 5% maximum interstory drift, which is the drift that was chosen in previous similar FEMA P-695 studies

for CC-PSW/CF. However, because all the archetypes considering uncoupled walls must resist seismic demand without the added benefit of ductile coupling beams, to be more conservative, the CMR was calculated here based on the response values obtained at 3% drift for each archetype. In other words, reaching a drift of 3% was defined as collapse for purposes of this FEMA P-695 study. However, results both at 3% and 5% maximum interstory drift were provided, for comparison purpose.

Based on the FEMA P695 methodology, all archetypes satisfied the specified performance requirement. Considering a "good" rating for total system collapse uncertainty (β_{TOT}), which is obtained by combining uncertainty factors related to record-to-record (β_{RTR}), design requirements (β_{DR}), test data (β_{TD}), and nonlinear modeling (β_{MDL}), all archetypes passed the $ACMR_{20\%}$ threshold for individual ACMR values of each archetype, and the $ACMR_{10\%}$ threshold for average of ACMR values in a performance group, both for the 3% and 5% maximum interstory drift criteria. In an average sense, the AMCR results at 5% maximum interstory drift are 28% and 31% larger for the planar and C-shaped archetypes, respectively, compared to the case where a 3% maximum interstory drift was considered as the response limit.

Data Availability Statement

Some or all data, models, or code that support the findings of this study are available from the corresponding author upon reasonable request.

Acknowledgments

This research was performed as an extension of the work testing C- and T-shaped C-PSW/CF and developing new seismic response factors (R-factors) for coupled C-PSW/CF that was conducted with support from the Charles Pankow Foundation (CPF) and the American Institute of Steel Construction (AISC), through CPF Research Grant #05-17 awarded to co-PIs Michel Bruneau, from University at Buffalo and Amit H. Varma, from Purdue University. Approach and methodologies approved in these previous studies were re-used here. Therefore, the authors are again grateful to members of the Peer Review Panel of these prior projects [Gregory G. Deierlein, Professor, Stanford University; Ron Klemencic, Chairman & CEO, Magnusson Klemencic Associates (MKA); and Rafael Sabelli, Principal and Director of Seismic Design, Walter P. Moore], and members of the Project Advisory Team [Larry Kruth, Vice President, American Institute of Steel Construction (AISC); John D. Hopper, Senior Principal/Director of Earthquake Engineering, MKA; Jim Malley, Senior Principal, Degenkolb Engineers; Bonnie Manley, Regional Director of Construction Codes and Standards, American Iron and Steel Institute (AISI); and Tom Sabol, Principal, Englekirk Institutional] as their technical guidance was valuable in formulating the methodology re-used for this current study on uncoupled walls.

References

Agrawal, S., M. Broberg, and A. H. Varma. 2020. *Seismic design coefficients for SpeedCore or composite plate shear walls/concrete filled (C-PSW/CF)*. Bowen Laboratory Research Rep. West Lafayette, IN: Purdue Univ.

AISC (American Institute of Steel Construction). 2016. *Seismic provisions for structural steel buildings*. ANSI/AISC 341-16. Chicago: AISC.

ASCE. 2016. *Minimum design loads for buildings and other structures*. ASCE 7-16. Chicago: ASCE.

Bruneau, M., A. H. Varma, E. Kizilarslan, M. Broberg, S. Shafaei, and J. Seo. 2019. "R-factors for coupled composite plate shear walls/concrete filled (CC-PSW/CF)." Accessed May 15, 2020. https://www.aisc.org/globalassets/aisc/research-library/pankow-aisc-r-factor-final-report-2019-07-19_submitted-revised-cover-page.pdf.

FEMA. 2008. *Quantification of building seismic performance factors*. FEMA P695. Washington, DC: Applied Technology Council, FEMA.

Kenarangi, H., E. Kizilarslan, and M. Bruneau. 2021. "Cyclic behavior of C-shaped composite plate shear walls—Concrete filled." *Eng. Struct.* 226 (Jan): 111306. https://doi.org/10.1016/j.engstruct.2020.111306.

Kizilarslan, E. 2021. "Experimental and analytical inelastic behavior of C- and T-shaped composite plate shear walls/concrete-filled (C-PSW/CF)." Ph.D. dissertation, Dept. of Civil, Structural and Environmental Engineering, State Univ. of New York at Buffalo.

Kizilarslan, E., M. Broberg, S. Shafaei, A. H. Varma, and M. Bruneau. 2021a. "Non-linear analysis models for composite plate shear walls-concrete filled (C-PSW/CF)." *J. Constr. Steel Res.* 184 (Sep): 106803. https://doi.org/10.1016/j.jcsr.2021.106803.

Kizilarslan, E., M. Broberg, S. Shafaei, A. H. Varma, and M. Bruneau. 2021b. "Seismic design coefficients and factors for coupled composite plate shear walls/concrete filled (CC–PSW/CF)." *Eng. Struct.* 244 (Oct): 112766. https://doi.org/10.1016/j.engstruct.2021.112766.

Kizilarslan, E., and M. Bruneau. 2023. "Cyclic behavior of T-shaped composite plate shear walls concrete filled." *J. Struct. Eng*.

Kurt, E. G., A. H. Varma, S. Epackachi, and A. S. Whittaker. 2015. "Rectangular SC wall piers: Summary of seismic behavior and design." In *Proc., Structures Congress 2015*, 1042–1051. Reston, VA: ASCE.

Lignos, D. 2008. "Sidesway collapse of deteriorating structural systems under seismic excitations." Doctoral dissertation, Dept. of Civil and Environmental Engineering, Stanford Univ.

McKenna, F., S. Mazzoni, and G. Fenves. 2016. *Open system for earthquake engineering simulation (OpenSees) software version 2.2.5*. Berkeley, CA: Univ. of California.

Neuenhofer, A., and F. C. Filippou. 1997. "Evaluation of nonlinear frame finite element models." *J. Struct. Eng.* 123 (7): 958–966. https://doi.org/10.1061/(ASCE)0733-9445(1997)123:7(958).

PEER (Pacific Earthquake Engineering Center). 2010. *Guidelines for performance-based seismic design of tall buildings*. PEER Rep. No. 2010/05. Berkeley, CA: Univ. of California.

PEER (Pacific Earthquake Engineering Research Center). 2017. *PEER NGA database*. Berkeley, CA: Univ. of California.

Rodgers, J. E., and S. A. Mahin. 2006. "Effects of connection fractures on global behavior of steel moment frames subjected to earthquakes." *J. Struct. Eng.* 132 (1): 78–88. https://doi.org/10.1061/(ASCE)0733-9445(2006)132:1(78).

Shafaei, S., A. H. Varma, J. Seo, and R. Klemencic. 2021. "Cyclic lateral loading behavior of composite plate shear walls/concrete filled." *J. Struct. Eng.* 147 (10): 04021145. https://doi.org/10.1061/(ASCE)ST.1943-541X.0003091.

Susantha, K. A. S., H. Ge, and T. Usami. 2001. "Uniaxial stress–strain relationship of concrete confined by various shaped steel tubes." *Eng. Struct.* 23 (10): 1331–1347. https://doi.org/10.1016/S0141-0296(01)00020-7.